www.czasopisma.pan.pl PAN POLSKA AKADEMIA NAUK www.journals.pan.pl

Arch. Metall. Mater. **68** (2023), 4, 1555-1562

DOI: https://doi.org/10.24425/amm.2023.146222

RUI-BIN GOU[1], WEN-JIAO DAN[1*], YONG-SHENG XU[2], MIN YU[3], TONG-JIE LI[1]

STRAIN-HARDENING PREDICTION OF DP600 STEEL CONSIDERING THE HETEROGENEOUS DEFORMATION BETWEEN FERRITE AND MARTENSITE

Dual-phase steels have received extensive attention in autobody frame manufacturing due to the resulting characteristics of an interesting combination of ductile ferrite and hard martensite. Moreover, the ductile ferrite and hard martensite lead to heterogeneous deformation in the boundary between the two phases. Then, geometrically necessary dislocations (GNDs) are created to accommodate a lattice mismatch due to the deformation incompatibility of the boundary in straining. In this study, a new empirical GND model is developed, in which the GND density is a function of local plastic deformation; the GND density is distributed in the phase boundary in accordance with an "S" model of material plastic strain. The boundary conditions are applied to define the parameters. The proposed model is verified with DP600 steel. The effects of the GNDs and the width between ferrite and martensite on the strain hardening of DP600 steel are evaluated.

Keywords: Strain-hardening model; DP600; GNDs; heterogeneous deformation; mechanical behaviors

1. Introduction

Dual-phase (DP) steels, considered as a typical advanced-high-strength steel, have received extensive attention in autobody frame manufacturing processes. This phenomenon is due to the results of an interesting combination of ductile ferrite and hard martensite, which promotes high work hardening and good ductility characteristics [1-2].

Appealing microstructures in DP steels have been focused on in different manners. First, the production processes are controlled to obtain better microstructures. To obtain ferrite and martensite, one method is hot rolling by controlling the final rolling temperature and cooling rate [3]. The other method is cold rolling to control the microstructure distribution with inter-critical annealing [4]. For a better understanding of the mechanical behaviors of ductile-ferrite and hard-martensite DP steels, various studies have been developed through experimental and theoretical models. The local strains of microstructures are measured by using Optical-Microscope (OM) [5, 6], Scanning-Electron-Microscope (SEM) and Electron-Backscattered-Diffraction (EBSD) [1,7-8] methods, and they are calculated by digital image correlation (DIC).

The strain-hardening characteristics of DP steels are dependent on the grain sizes and martensitic volume fractions of the materials. The reduction in the grain sizes of metallic alloys can improve the strength [9]; in particular, the refinement of ferrite grains is found to be quite effective in enhancing material behaviors [10]. The fine martensite particles increase the strain hardening and ductility characteristics of ultrafine-grained DP steel [11] and a uniform distribution of microstructure results in the superior tensile properties of steels [12]. The high martensitic volume fraction in DP steel can significantly improve the strength and subsequently reduce the elongation [13,14]. The local topography [15], stress triaxiality [16] and strain partition [17] of martensite affect the work hardening stage [18], damage and crack behaviors [19], cycle fatigue life [20] and formability [21].

However, the overall strain of the material is between the martensite strain and ferrite strain [6]; this phenomenon leads to heterogeneous deformation in the boundary between the soft ferrite and hard martensite. Then, geometrically necessary dislocations (GNDs) are created to accommodate a lattice mismatch due to the deformation incompatibility of the boundary during strain. A proposed model of GNDs with plastic deformation is introduced by Nye [22] and Ashby [23] and further developed

[1] ANHUI SCIENCE AND TECHNOLOGY UNIVERSITY, COLLEGE OF MECHANICAL ENGINEERING, FENGYANG 233100, ANHUI, CHINA
[2] SHANGHAI JIAO TONG UNIVERSITY, DEPARTMENT OF ENGINEERING MECHANICS, SCHOOL OF NAVAL ARCHITECTURE, OCEAN AND CIVIL ENGINEERING, SHANGHAI 200240, CHINA
[3] ANHUI SCIENCE AND TECHNOLOGY UNIVERSITY, COLLEGE OF ARCHITECTURE, BENGBU 233000, ANHUI, CHINA
* Corresponding author: danwj017@163.com

by Needleman et al. [24-25] and Nix et al. [26], successively. The GNDs effects on the material strain-hardening have been measured and predicted extensively in the literature [27-32]. The local heterogeneous deformation characteristics in the boundaries between the two phases are complex, and a strain gradient is introduced to calculate the GNDs [26,33].

In this study, the characteristics of strain-hardening of DP steels are predicated with the effects of GNDs in the boundary between two phases. A new empirical GND model is developed, in which GND density is a function of local plastic deformation, which is distributed in the phase boundary with an "S" model of material plastic strain. The parameters are defined using boundary conditions. The impact of parameter δ named Ferrite–Martensite (F–M) boundary width on the strain-hardening of the material are discussed.

2. Theoretical model

2.1. Heterogeneous deformation between ferrite and martensite

As a principal element, carbon usually segregates heterogeneously at the grain boundaries [34]. Especially, carbon content shows a gradient decrease from Martensite to Ferrite in DP steels [35]. The solute carbon induces the lattice mismatch at the grain boundaries, and the local mechanical behaviors (e.g., nanohardness) between Martensite to Ferrite decreases gradually [28]. The gradient reduction of the local nanohardness results in the corresponding plastic strain at the grain boundaries in bi-crystal changes similarly during the deformation process, and the local GNDs improve [36,37]. In other words, we can assume the mechanical behaviors of martensite-ferrite DP steels is homogeneous and the features at the grain boundaries is gradient reduction from Martensite to Ferrite continuously. Then the average strain replaces the Martensite and Ferrite deformation and a function reducing from Ferrite to Martensite, replaces the strain distribution at the grain boundaries.

The microstructure strain ε_i given in Eq. (1) is linear to the total strain of material ε [37].

$$\varepsilon_i = K_i \varepsilon \tag{1}$$

where i is the ferrite (F)/martensite (M) phase, K_i is the strain factor, and $K_F > 1 > K_M > 0$.

The strain between the two phases (F–M boundary with thickness δ) is non-linear to the total strain of the material and increases from ε_M to ε_F. The strain gradient of the F–M boundary is equal to that of martensite at the beginning, then it increases to a maximum value and finally reduces to that of ferrite (Fig. 1). Eq. (2) is the relationship between the strain of the boundary ε_{FM} and the total strain of material ε.

$$\varepsilon_{FM} = \frac{a}{1+b\exp(-kx)}\varepsilon,\ (0 \le x \le \delta) \tag{2}$$

where the parameters a, b and k are defined by three boundary conditions: 1) $x = 0$, $\varepsilon_{FM} = \varepsilon_M$; 2) $x = \delta$, $\varepsilon_{FM} = \varepsilon_F$ and 3) $x = \delta'$, $\frac{\partial^2 \varepsilon_{FM}}{\partial x^2} = 0$. The parameter δ' is assumed to be $\delta/2$ in this study.

The GNDs ρ_G (Eq. (3)) are described as follows with the Ashby model [23]:

$$\rho_G = \frac{1}{b}\frac{\partial \gamma_{FM}}{\partial x} = \frac{M}{b}\cdot\frac{\partial \varepsilon_{FM}}{\partial x} = \\ = \frac{M}{b}\cdot\frac{a\cdot b\cdot k\cdot\exp(-kx)}{(1+b\cdot\exp(-kx))^2}\cdot\varepsilon,\ (0 \le x \le \delta) \tag{3}$$

where M and b refer to the Taylor factor and the Burgers vector, respectively. γ_{FM} is the shear strain of the F–M boundary.

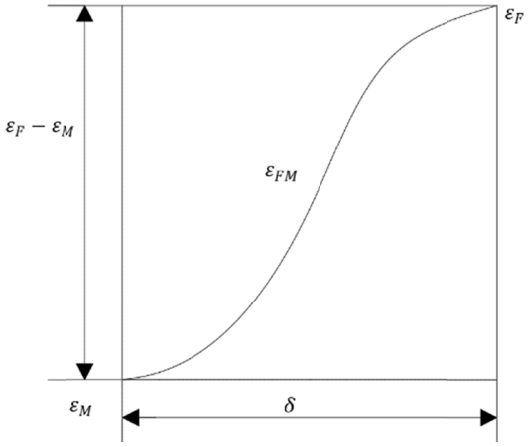

Fig. 1. Scheme of heterogeneous deformation between ferrite and martensite

2.2. Strain hardening model

By considering the mixture hardening law [38], the strain hardening model of DP steel considering GNDs can be expressed as Eq. (4).

$$\sigma = V_M K_M \sigma_M + (V_F - V_{FM}) K_F \sigma_F + \\ + V_{FM} K_{FM} \sigma_{FM} \tag{4}$$

where V_M, V_F and V_{FM} are the volume fractions of M, F and F–M, respectively; K_M, K_F and K_{FM} are their strain factors, respectively; σ_M, σ_F and σ_{FM} are their equivalent stress, respectively.

The relationship between the material strain ε and the phase strain ε_i [37] is given in Eq. (5), as follows:

$$\varepsilon = V_M K_M \varepsilon_M + (V_F - V_{FM}) K_F \varepsilon_F + \\ + V_{FM} K_{FM} \varepsilon_{FM} \tag{5}$$

where ε_M, ε_F and ε_{FM} are the strains of F, M and F–M, respectively.

In the model (Eq. (5)), martensite assumed as a circular with a diameter of d_M and uniformly distributed in the ferrite matrix. The interaction part between ferrite and martensite boundary is defined as F–M and the F–M thickness is δ of F–M. By the area comparison, the V_{FM} can be expressed by parameters δ (the F–M

thickness), V_M (the volume fractions of M) and d_M (the grain size of M), respectively. As given in Eq. (6):

$$V_{FM} = \left(\frac{4\delta}{d_M} + \left(\frac{2\delta}{d_M} \right)^2 \right) V_M \tag{6}$$

Based on the Eq. (5), The strain factor of F–M can be calculated from Eq. (7):

$$K_{FM} = \frac{1 - \left(V_M K_M + \left(V_F - V_{FM} \right) K_F \right)}{V_{FM}} \tag{7}$$

The stress of M, F and F–M can be expressed as Eq. (8), Eq. (9) and Eq. (10), respectively [39].

$$\sigma_M = \sigma_{M0} + \alpha M G_M b \sqrt{\rho_M} \tag{8}$$

$$\sigma_F = \sigma_{F0} + \alpha M G_F b \sqrt{\rho_F} \tag{9}$$

$$\sigma_{FM} = \sigma_{F0} + \alpha M G_F b \sqrt{\rho_F + \rho_G} \tag{10}$$

where σ_{M0}, G_M and ρ_M are the initial stress, shear modulus and dislocation density of M, respectively; α is an empirical material parameter [40]. σ_{F0}, G_F and ρ_F are the initial stress, shear modulus and dislocation density of F, respectively [29-32]. ρ_G is the GND of the F–M boundary and it can be calculated from Eq. (3).

For F and M, their dislocation density changes are given in Eq. (11) and Eq. (12) [39,41], respectively.

$$\frac{d\rho_F}{d\varepsilon} = M K_F \left[\frac{1}{b} \left(\frac{k_{F0}}{d_F} + k_{F1} \sqrt{\rho_F} \right) - k_{F2} \rho_F \right] \tag{11}$$

$$\frac{d\rho_M}{d\varepsilon} = M K_M \left[\frac{1}{b} \left(\frac{k_{M0}}{d_M} + k_{M1} \sqrt{\rho_M} \right) - k_{M2} \rho_M \right] \tag{12}$$

where k_{F0}, k_{F1} and k_{F2} are material parameters of F. k_{M0}, k_{M1} and k_{M2} are material parameters of M, and parameters d_F and d_M are the grain size of F and M, respectively.

3. Material and experiment

The DP600 was chosen to evaluate the proposed model. The thickness of the steel sheet was 0.9 mm. Fig. 2 is a metallographic picture of DP600. TABLE 1 and TABLE 2 are separately the chemical compositions and the mechanical properties of the investigated steel. According to the photomicrograph, we obtained V_M = 23.33%, V_F = 76.67%, d_M = 4.2 μm and d_F = 8.4 μm. The strain factor of the microstructure was calculated from the photomicrograph with plant input mapping (PIM) [6] (in Fig. 3 and TABLE 3). The experimental methods and equipment can be found in Ref. [6].

TABLE 1

Chemical compositions of DP600 steel (wt.%)

Material	C	Cr	Cu	Mn	Mo	Ni	P	Si	S
DP600	0.138	0.041	0.012	0.927	0.001	0.031	0.008	0.441	0.003

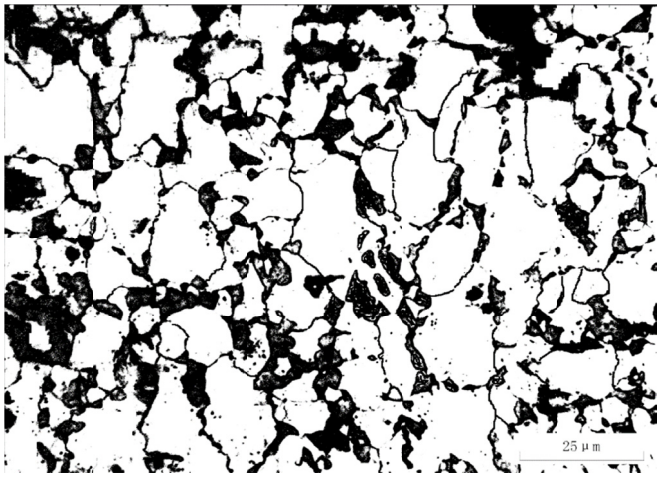

Fig. 2. Metallographic picture of DP600 steel (black: martensite, white: ferrite)

TABLE 2

Mechanical properties of DP600 steel

Material	Yield strength/MPa	Ultimate tensile strength/MPa	Total elongation/%
DP600-#1	338.7	668.2	25.9
DP600-#2	342.6	707.2	22.8
DP600-#3	324.5	674.0	22.6
Average	335.3	683.1	23.8

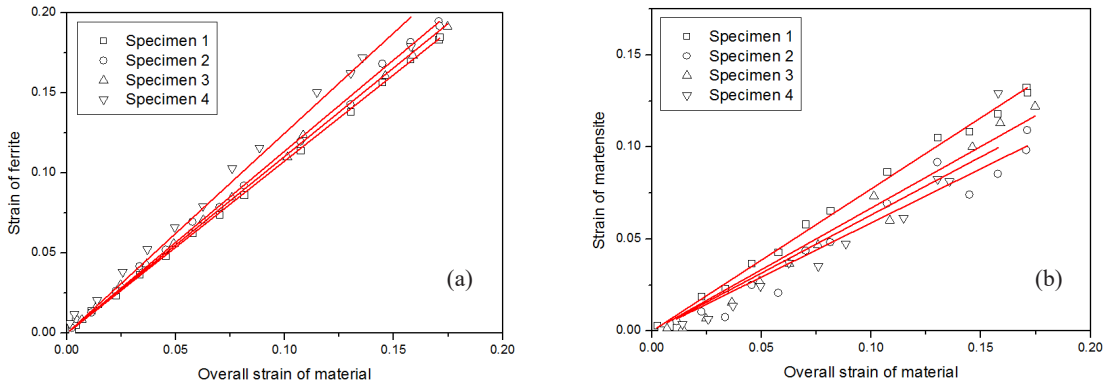

Fig. 3. Strain of F-phase and M-phase: (a) F and (b) M

TABLE 3

Strain factors of ferrite and martensite for DP600 steel

Specimen	1#	2#	3#	4#	Average
F	1.076	1.137	1.107	1.250	1.1425
M	0.772	0.587	0.668	0.631	0.6645

4. Results and discussion

The parameters of the proposed model are given in Tables 4-6. Parameters in TABLE 4 are the experimental results of the research group mainly to describe the microstructure features of *F*, *M* and *F*–*M*. Parameters in TABLE 5 are referenced from the literatures mainly focused on the calculation of strain hardening of material. The TABLE 6 gives the empirical parameters related to the dislocation evolution.

The proposed model is verified by a comparison with the experimental results (in Fig. 4). Fig. 5 and Fig. 6 show the effects of the GNDs and *F*–*M* width on the mechanical behaviors, respectively. The material hardening rate *H* and strain-hardening exponent *n* are calculated as $H = \frac{d\sigma}{d\varepsilon}$ and $n = \frac{d\sigma}{d\varepsilon} \cdot \frac{\varepsilon}{\sigma}$, respectively.

TABLE 4

Parameters for microstructure features of the DP600 steel

Parameters	d_F (μm)	d_M (μm)	δ (μm)	V_M (%)	V_F (%)	K_F	K_M	K_{FM}
DP600	8.4	4.2	0.84	23.33	76.67	1.1425	0.6645	0.839

TABLE 5

Parameters of the strain hardening model [5,6,32,34]

Parameters	α	M	b (m^{-2})	G_F (GPa)	G_M (GPa)	σ_{F0} (MPa)	σ_{M0} (MPa)	g_M, g_F
DP600	0.33	3.0	1.0×10^{-10}	72	78.5	315	650	0.13

TABLE 6

Parameters for the dislocation evolution of microstructure

Parameters	k_{i0}	k_{i1}	k_{i2}
F	0.13	1.137	1.107
M	0.13	0.587	0.668

From Fig. 4(a)-(c), the proposed model could describe the mechanical behaviors very well. The results showed the *M*-phase improved the material strength; the *F*-phase provided the ductility of the material; the *F*–*M* boundary introduced heterogeneous deformation to maintain the deformation compatibility between the hard and soft phases and the GNDs were created to accommodate a lattice mismatch due to the deformation incompatibility of the boundary during strain; this phenomenon induced the local strength of the *F*–*M* boundary to be larger than the strength of *F*-phase; and the local strain was higher than that of martensite and lower than that of ferrite (Fig. 4(d))

The local GNDs improved the strength of DP600 due to the local lattice mismatch of the *F*–*M* boundary (in Fig. 5(a)). Both parameters *H* and *n* improved due to the local heterogeneous deformation to maintain the deformation compatibility between the hard (*M*) and soft (*F*) phases (in Fig. 5(b) and (c)). The martensite dislocation density was over 10^{16} m^{-2} at high strain,

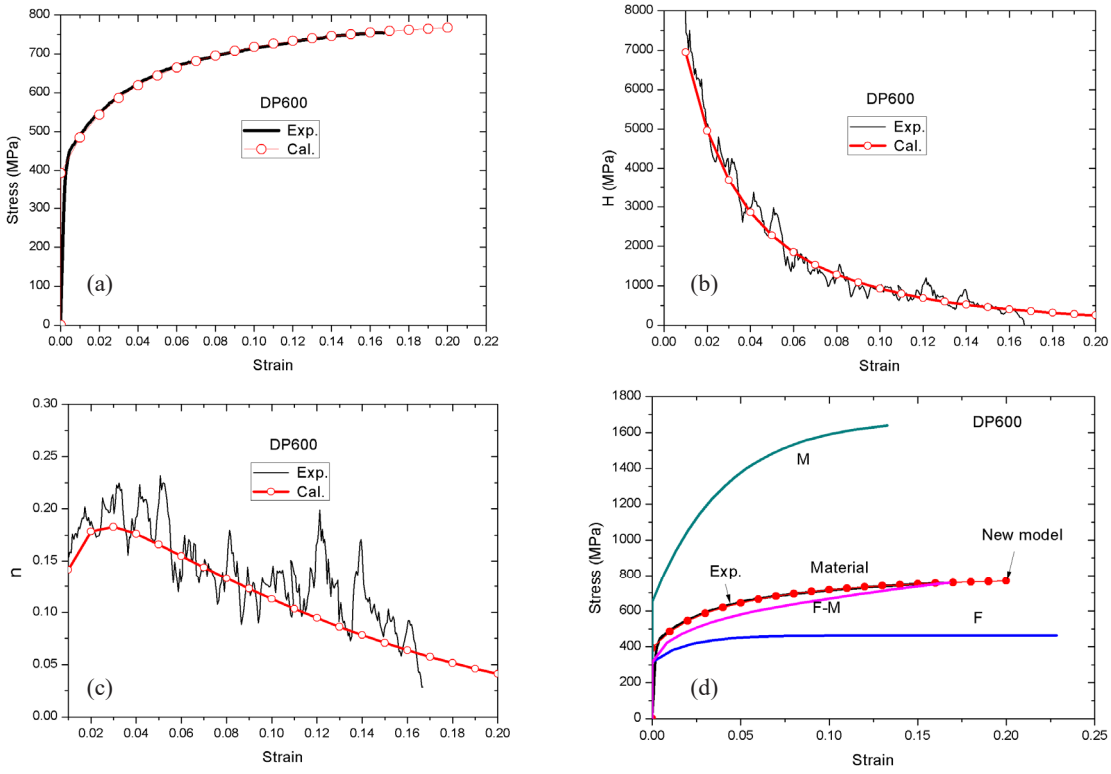

Fig. 4. New Model verification: (a) stress-strain curve of material, (b) *H* (Hardening rate), (c) *n* (Strain-hardening exponent) and (d) stress-strain curves of each phase

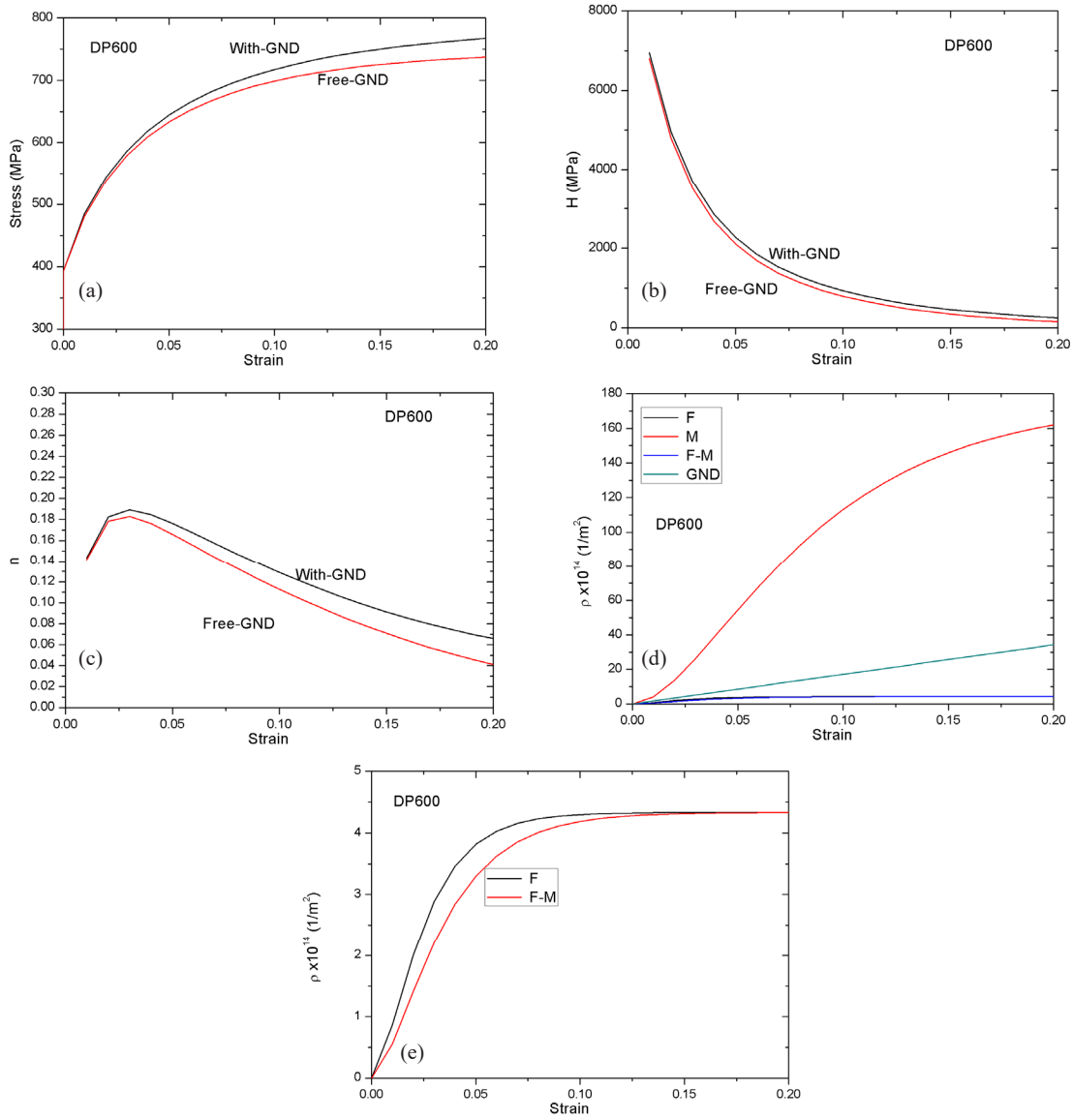

Fig. 5. Effects of the GNDs on the mechanical behaviors of DP600: (a) stress-strain curve, (b) H, (c) n, (d) dislocation density of each phase and (e) dislocation density of F and F–M

that of ferrite was approximately 4.0×10^{14} m^{-2} and the GND density of FM was higher than 2.0×10^{15} m^{-2} (Fig. 5(d)). Ferrite improved the strength of the material before the strain at 0.1, but its dislocation evolution reached a balance after the strain at 0.1, indicating that the generation and annihilation rates of ferrite dislocation were equal. The statistically stored dislocations of the F–M boundary were similar to those of ferrite, although the increment of dislocation density was lower than that of ferrite before strain at 0.1 (in Fig. 5(e)).

The strength of DP600 improved with the F–M boundary width δ. The stress decreased with decreasing width due to the dislocation density decreasing but the F–M boundary volume fraction improved the material strength (in Fig. 6(a)-(c) and TABLE 7). The hardening rate, strain-hardening exponent and necking point increased with increasing width of the F–M boundary (in Fig. 6(d)-(e)) and the necking point at $\delta = 0.3d_M$ was 0.1181, which was consistent with the experimental results (in Fig. 6(f)). The width of the F–M boundary was approximately $0.25d_M$, as measured by Ramazani et al. [30,32,42], but the layer size could be predicted to be 0.3 d_M considering the GND density of the inner part of each phase.

TABLE 7

Parameter changes due to the width of the F–M boundary

Parameters	$\delta = 0.10d_M$	$\delta = 0.15d_M$	$\delta = 0.20d_M$	$\delta = 0.25d_M$	$\delta = 0.3d_M$
V_{FM} (%)	4.89	7.51	10.25	13.10	16.10
K_{FM}	0.511	0.732	0.839	0.893	0.950

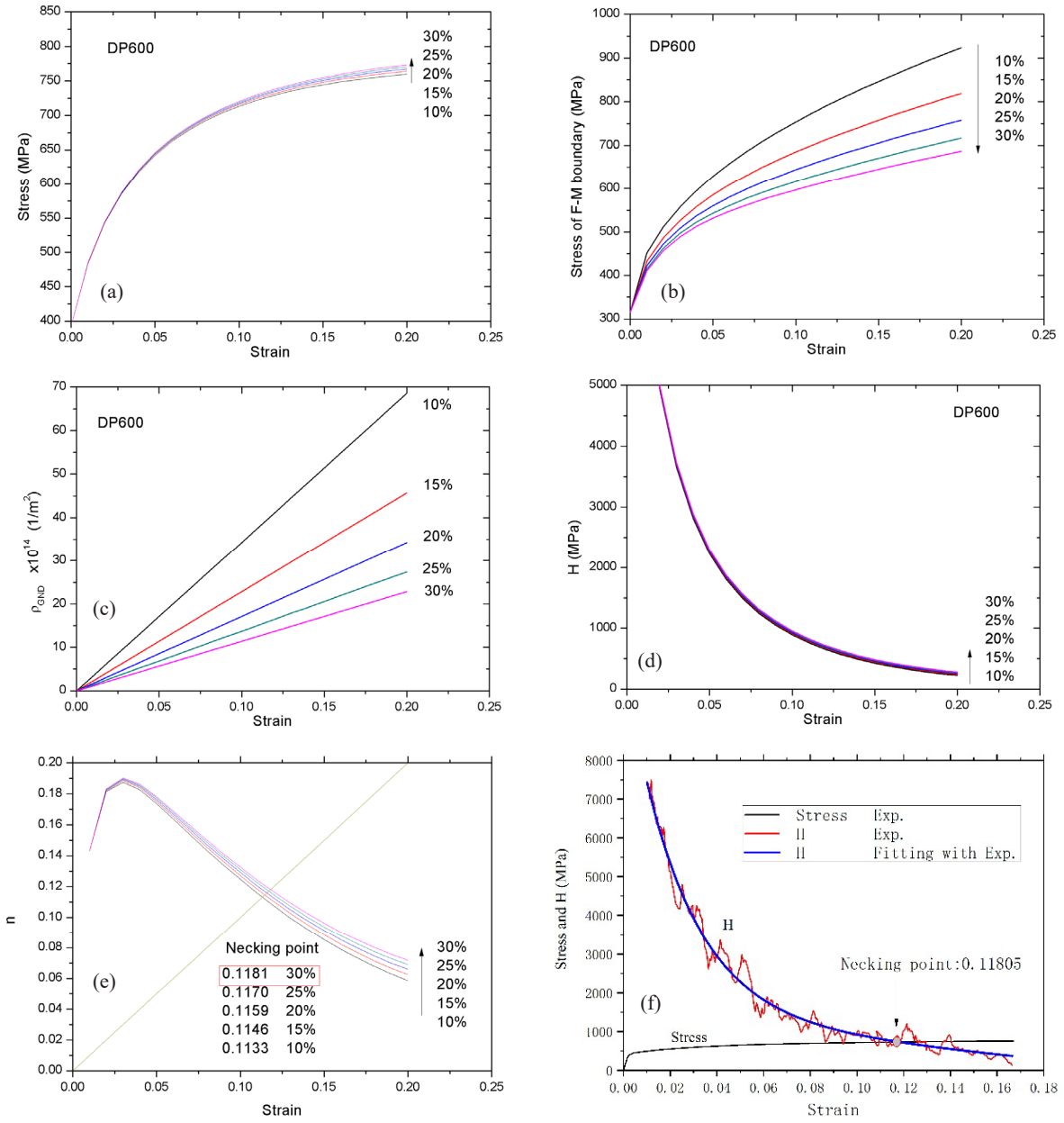

Fig. 6. Effects of *F–M* width on the mechanical behaviors of DP600: (a) stress-strain curve, (b) stress with *F–M* width, (c) dislocation density with *F–M* width, (d) *H* with *F–M* width, (e) *n* with *F–M* width and (f) necking point of DP600

5. Conclusion

In this paper, a strain-hardening model for ferrite-martensite DP steel is developed considering heterogeneous deformation between the two phases. The new model is verified with DP600 steel. The effects of GNDs and the width between the two individual phases on the strain-hardening of DP600 steel are evaluated. The main conclusions are as follows:

A new empirical GND model is developed, in which a function of local plastic deformation was employed to define the GND density distributed in the phase boundary with an "S" model of material plastic strain. The boundary conditions are applied to define the parameters. The proposed model is verified with DP600 steel.

The effects of GNDs (heterogeneous deformation between *F* and *M*) on the strain-hardening characteristics of the material are discussed. The results point that the local strength of *F–M* is higher than that of ferrite and the local strain is larger than martensite strain but smaller than ferrite strain. The martensite dislocation density is over 10^{16} at high strain, that of ferrite is approximately 4.0×10^{14} and the GND density of *F–M* is larger than 2.0×10^{15}.

The strength of DP600 improves with the width of the *F–M* boundary and the stress decreases with its width due to the dislocation density decreasing, but its volume fraction V_{FM} improves the material strength. When the width of the *F–M* boundary increases, parameters *H* and *n* increase. Moreover, necking point also increase and the necking point at $\delta = 0.3d_M$ is 0.1181, which is in good agreement with the experimental results.

Acknowledgements

This work was jointly supported by the Anhui university provincial natural science research projects (No. 2022AH051630, No. KJ2021ZD0111 and No. KJ2021A0862), and Anhui province natural science foundation (No. 2108085ME167).

REFERENCES

[1] C.C. Tasan, M. Diehl, D. Yan et al., An Overview of Dual-Phase Steels: Advances in Microstructure Oriented Processing and Micromechanically Guided Design, Annu. Rev. Mater. Res. **45** (1), 91-431 (2015).

[2] T. Sirinakorn, S.Wongwises, V. Uthaisangsuk, A Study of Local Deformation and Damage of Dual Phase Steel, Mater. Des. **64**, 729-742 (2014).

[3] H. Balmori-Ramirez, J.G. Cabañas-Moreno, H.A. Calderon-Benavides, et al., Austenite-Ferrite Transformation in Hot Rolled Mn-Cr-Mo Dual Phase Steels, Mater. Sci. Forum **560**, 79-84 (2007).

[4] P.R. Mould, An Overview of Continuous-Annealing Technology for Steel Sheet Products, JOM. **34** (5), 18-28 (1982).

[5] C. Ren, W.J. Dan, W.G. Zhang, Effects of ferrite grain characteristics on strain distribution of dual-phase steel, Mater. Res. Express **6**, 016539 (2019).

[6] T.T. Huang, R.B. Gou, W.J. Dan, W.G. Zhang, Strain-Hardening Behaviors of Dual Phase Steels with Microstructure Features, Mater. Sci. Eng. A **672**, 88-97 (2016).

[7] C.C. Tasan, J.P.M. Hoefnagels, E.C.A. Dekkers, M.G.D. Geers, Multi-axial deformation setup for microscopic testing of sheet metal to fracture, Exp. Mech. **52**, 669-678 (2012).

[8] H. Ghadbeigi, C. Pinna, S. Celotto, J.R, Yates, Local plastic strain evolution in a high strength dual-phase steel, Materials Science and Engineering A **527**, 5026-32 (2010).

[9] M. Delince, P.J. Jacques, T. Pardoen, Separation of size-dependent strengthening contributions in fine-grained Dual Phase steels by nanoindentation, Acta Materialia **54**, 3395-3404 (2006).

[10] M. Zamani, H. Mirzadeh, H.M. Ghasemi, Dependency of Natural Aging on the Ferritfoe Grain Size in Dual-Phase Steel, Metallurgical and Materials Transactions A **50A**, 4961-4964 (2019).

[11] N. Saeidi, F. Ashrafizadeh, B. Niroumand, Development of a new ultrafine grained dual phase steel and examination of the effect of grain size on tensile deformation behavior, Metallurgical and Materials Transactions A **599**, 145-149 (2014).

[12] H. Seyedrezai, A.K. Pilkey, J.D. Boyd, Effects of martensite particle size and spatial distribution on work hardening behavior of fine-grained dual-phase steel, Canadian Metallurgical Quarterly **57**, 28-37 (2018).

[13] S. Kumar, A. Kumar, R. Sah, et al., Mechanical and Electrochemical Behavior of Dual-Phase Steels Having Varying Ferrite-Martensite Volume Fractions, Journal of Materials Engineering and Performance **28**, 3600-3613 (2019).

[14] Q.Q. Lai, L. Brassart, O. Bouaziz, et al., Influence of martensite volume fraction and hardness on the plastic behavior of dual-phase steels: Experiments and micromechanical modeling, International Journal of Plasticity **80**, 187-203 (2016).

[15] V.F. Rad, R. Khamedi, A.R. Moradi, The effect of martensite volume fraction on topography of dual phase steels, Materials Letters **239**, 21-23 (2019).

[16] S.K. Paul, Effect of martensite volume fraction on stress triaxiality and deformation behavior of dual phase steel, Materials & Design **50**, 782-789 (2013).

[17] A.K. Rana, S.K. Paul, P.P. Dey, et al., Effect of Martensite Volume Fraction on Strain Partitioning Behavior of Dual Phase Steel, Physical Mesomechanics **21**, 333-340 (2018).

[18] H.R. Pakzaman, S.S.G. Banadkouki, Effect of martensite volume fraction on abnormal work hardening behavior of a low carbon low alloy ferrite-martensite dual-phase steel, International Journal of Materials Research **111**, 983-994 (2020).

[19] Q.Q. Lai, O. Bouaziz, M. Goune, et al., Damage and fracture of dual-phase steels: Influence of martensite volume fraction, Materials Science and Engineering A **646**, 322-331 (2015).

[20] S.K. Paul, N. Stanford, T. Hilditch, Effect of martensite volume fraction on low cycle fatigue behaviour of dual phase steels: Experimental and microstructural investigation, Materials Science and Engineering A **638**, 296-304 (2015).

[21] M. Zaeimi, A. Basti, M. Alitavoli, Effect of Martensite Volume Fraction on Forming Limit Diagrams of Dual-Phase Steel, Journal of Materials Engineering and Performance **24**,1781-1789 (2015).

[22] J.F. Nye, Some geometrical relations in dislocated crystals, Acta Metall. **1**5, 153-162 (1953).

[23] M.F. Ashby, The deformation of plastically non-homogeneous materials, Philos. Mag. **21**, 399-424 (1970).

[24] A. Needleman, J. Gil Sevillano, Preface to the viewpoint set on: geometrically necessary dislocations and size dependent plasticity, Scr. Mater. **48**, 109-111 (2003).

[25] E. Van der Giessen, A. Needleman, GNDs in nonlocal plasticity theories: lessons from discrete dislocation simulations, Scr. Mater. **48**, 127-132 (2003).

[26] W.D. Nix, H. Gao, Indentation size effects in crystalline materials: A law for strain gradient plasticity, Mech. Phys. Solids **46**, 411-425 (1998).

[27] M. Calcagnotto, D. Ponge, E. Demir, et al., Orientation gradients and geometrically necessary dislocations in ultrafine grained dual-phase steels studied by 2D and 3D EBSD, Materials Science and Engineering A **527**, 2738-2746 (2010).

[28] J. Kadkhodapour, S. Schmauder, D. Raabe, et al., Experimental and numerical study on geometrically necessary dislocations and non-homogeneous mechanical properties of the ferrite phase in dual phase steels, Acta Materialia **59**, 4387-4394 (2011).

[29] A. Ramazani, K. Mukherjee, U. Prahl, et al., Transformation-Induced, Geometrically Necessary, Dislocation-Based Flow Curve Modeling of Dual-Phase Steels: Effect of Grain Size, Metallurgical and Materials Transactions A **43**, 3850-3869 (2012).

[30] A. Ramazani, K. Mukherjee, A. Schwedt, et al., Quantification of the effect of transformation-induced geometrically necessary dislocations on the flow-curve modelling of dual-phase steels, International Journal of Plasticity **43**, 128-152 (2013).

[31] A. Kundu, D.P. Field, Influence of plastic deformation heterogeneity on development of geometrically necessary dislocation density in dual phase steel, Materials Science and Engineering A **667**, 435-443 (2016).

[32] C. Ren, W.J. Dan, Y.S. Xu et al., Strain-Hardening Model of Dual Phase Steel with Geometrically Necessary Dislocations, Journal of Engineering Materials and Technology Transactions of the ASME **140**, 031009 (2018).

[33] H.J. Gao, Y.G. Huang, Geometrically Necessary Dislocation and Size-Dependent Plasticity, Scr. Mater. **48**, 113-118 (2013).

[34] Yuki Toji, Hiroshi Matsuda, Michael Herbig, Pyuck-Pa Choi, Dierk Raabe, Atomic-scale analysis of carbon partitioning between martensite and austenite by atom probe tomography and correlative transmission electron microscopy, Acta Materialia **65**, 215-228 (2014).

[35] HanSang Lee, Byoungchul Hwang, Sunghak Lee Chang Gil Lee, Sung-Joon Kim, Effects of Martensite Morphology and Tempering on Dynamic Deformation Behavior of Dual-Phase Steels, Metallurgical and Materials Transactions A **35**, 2371-2382 (2004).

[36] H. Liang, F.P.E. Dunne, GND accumulation in bi-crystal deformation: Crystal plasticity analysis and comparison with experiments, International Journal of Mechanical Sciences **51**, 326-333 (2009).

[37] S.K. Paul, M. Mukherjee, Determination of Bulk Flow Properties of a Material from the Flow Properties of its Constituent Phases, Comput. Mater. Sci. **84**, 1-12 (2014).

[38] W.J. Dan, Z.Q. Lin, S.H. Li, W.G. Zhang, Study on the Mixture Strain Hardening of Multi-Phase Steels, Mater. Sci. Eng. A **552**, 1-8 (2012).

[39] H. Mecking, U.F. Kocks, Kinetics of flow and strain-hardening [J]. Acta Metallurgica **29** (11), 1865-1875 (1981).

[40] G.I. Taylor, The Mechanism of Plastic Deformation of Crystals. Part I. Theoretical. Proceedings of the Royal Society of London. Series A, Containing Papers of a Mathematical and Physical Character V145 (855), 362-387 (1934).

[41] W.J. Dan, T.T. Huang, W.G. Zhang, A Multi-Phase Model for High Strength Steels, Int. J. Appl. Mechanics 07, 1550080 (2015).

[42] Gou Ruibin, Dan Wenjiao, Zhang weigang, et al., Research on flow behaviors of the constituent grains in ferrite-martensite dual phase steels based on nanoindentation measurements, Materials Research Express **4**, 076510 (2017).